



**HAL**  
open science

# Density functional theory study of structural, electronic and optical properties of cobalt-doped BaSnO<sub>3</sub>

Soukaina Chahib, Daniel Fasquelle, Gérard Leroy

## ► To cite this version:

Soukaina Chahib, Daniel Fasquelle, Gérard Leroy. Density functional theory study of structural, electronic and optical properties of cobalt-doped BaSnO<sub>3</sub>. *Materials Science in Semiconductor Processing*, 2022, 137, pp.106220. 10.1016/j.mssp.2021.106220 . hal-04459581

**HAL Id: hal-04459581**

**<https://ulco.hal.science/hal-04459581>**

Submitted on 22 Jul 2024

**HAL** is a multi-disciplinary open access archive for the deposit and dissemination of scientific research documents, whether they are published or not. The documents may come from teaching and research institutions in France or abroad, or from public or private research centers.

L'archive ouverte pluridisciplinaire **HAL**, est destinée au dépôt et à la diffusion de documents scientifiques de niveau recherche, publiés ou non, émanant des établissements d'enseignement et de recherche français ou étrangers, des laboratoires publics ou privés.



Distributed under a Creative Commons Attribution - NonCommercial 4.0 International License

## Density Functional Theory Study of Structural, Electronic and Optical Properties of Cobalt-Doped BaSnO<sub>3</sub>

S. Chahib<sup>1,2\*</sup>, D. Fasquelle<sup>2</sup> and G. Leroy<sup>2</sup>

<sup>1</sup>Laboratoire de Matière Condensée et Sciences Interdisciplinaires (LaMCScI), Faculty of Sciences, Mohammed V University, Rabat, Morocco

<sup>2</sup>Univ. Littoral Côte d'Opale, UR 4476, UDSMM, Unité de Dynamique et Structure des Matériaux Moléculaires, F-62228 Calais, France

\*Email address: s.chahib@gmail.com

**Abstract:** The physical properties of functional oxides can be fine-tuned by an appropriate dopant in the A and B sites of the perovskite lattice structure. In this study, cobalt (Co) was used as a dopant to investigate its influence on the structural, electronic, and optical properties of BaSnO<sub>3</sub> using density functional theory (DFT) within WIEN2K-code based on the generalized gradient approximation (GGA) and the modified Becke-Johnson exchange potential (mBJ). Calculations were performed for BaSn<sub>1-x</sub>Co<sub>x</sub>O<sub>3</sub> oxide with x = 0, 12.5, 25, 37.5 and 50 %. Analyses of the studied materials have revealed that the lattice parameter has linearly decreased from 4.171 Å (x = 0 %) to 4.069 Å (x = 50 %) upon increasing Co-doping concentration. Pure BaSnO<sub>3</sub> has an indirect energy bandgap (R-Γ) of 2.6 eV, while the valence band maximum (VBM) and the conduction band minimum (CBM) were both located in the Γ point of the Brillouin zone implying a direct energy bandgap for the Co-doped BaSnO<sub>3</sub>. Additionally, the optical energy bandgap was reduced by 46 % for x = 50 %. Moreover, the absorption coefficient has increased from around 1×10<sup>5</sup> cm<sup>-1</sup> (x = 0 %) to a maximum of about 6×10<sup>5</sup> cm<sup>-1</sup> in the UV band and 2.5×10<sup>5</sup> cm<sup>-1</sup> at the beginning of the visible band upon Co-doping (x = 50 %). The present study, therefore, shows that Co-doped BaSnO<sub>3</sub> is a very interesting material for the performance enhancement of oxides dedicated to photovoltaic and optoelectronic devices.

**Keywords:** Perovskites, BaSnO<sub>3</sub>, Electronic properties, Structural properties, optical properties and DFT.

## 1. Introduction

Lead-free oxide perovskite materials have been the centre of attention for various applications such as photocatalysis, electrocatalysis, supercapacitors, and photovoltaics [1]–[4]. Particularly, the exceptional properties make it a more feasible class of materials for the fabrication of photovoltaics. This is primarily attributed to their inherent properties such as oxygen stability, transparent to visible light with good electrical conductivity and high electronic mobility [5]–[8]. Among many perovskite structured materials, Barium Stannate,  $\text{BaSnO}_3$  (BSO) is considered as one of the promising materials for catalysis [9]–[11], temperature stable capacitors [12] and photovoltaics [13], [14].  $\text{BaSnO}_3$  perovskite crystallizes in a cubic structure at room temperature.  $\text{BaSnO}_3$  ceramic is n-type semiconductor with a large bandgap between 3.1 and 3.4 eV due to the large difference in electronegativity between oxygen and metallic ions, it is being considered as an alternative for the widely used binary oxide,  $\text{TiO}_2$  [13], [15]–[17]. Although  $\text{TiO}_2$  provides good optical transparency, its poor electron mobility limits its application in solar cells. Recently,  $\text{BaSnO}_3$  oxide is emerging as a transparent oxide conducting (TCO) layer for the solar cells [13].

Further, in order to improve the efficiency of  $\text{BaSnO}_3$  in technological aspects, doping is one of the most reliable strategies. Thus, many works have been reported so far by doping with some elements such as La [18]–[21], Gd [22], [23], Nb [24], Sb [15], [25] and Ge [26] to improve its properties for the transparent conducting oxide-based devices. Nevertheless, all these reported doping elements led to an increase in the bandgap energy of BSO material. However, the use of doping elements to reduce the bandgap has not yet been widely explored. Goa et al. [27] demonstrated experimentally that cobalt doping can lower the bandgap energy of  $\text{BaSnO}_3$ . When the cobalt dopant concentration was increased, the lattice parameter and bandgap energy of  $\text{BaSn}_{1-x}\text{Co}_x\text{O}_3$  ( $x = 0, 0.05, 0.10, 0.20, 0.35, \text{ and } 0.50$ ) thin films decreased. Recently Rajamanickam et al. [28] have studied the effect of cobalt on structural and optical properties of  $\text{BaSnO}_3$ , and they reported that the cobalt-doping can improve the photovoltaic performance of  $\text{BaSnO}_3$ .

The objective of this study is to investigate the influence of cobalt-doping on the structural, electronic, and optical properties of doped- $\text{BaSnO}_3$  using first principles calculations. The choice of this element for doping is motivated by the ionic radius of  $\text{Co}^{2+}$  (0.63 Å) is smaller than the ionic radius of  $\text{Sn}^{4+}$  (0.7 Å). Therefore, cobalt atoms can replace Sn atoms effectively in  $\text{BaSnO}_3$  lattice. In addition, the difference in the oxidation number of two electrons

between the  $\text{Co}^{2+}$  element and  $\text{Sn}^{4+}$ . The obtained results showed that the cobalt doping could reduce the band gap and ameliorate the absorption coefficient of  $\text{BaSnO}_3$ .

The first principles density functional theory (DFT) calculation is an efficient route to investigate the physical properties of materials. Various theoretical calculations have been adopted to understand the electronic and optical properties of  $\text{BaSnO}_3$  [29]–[31]. S. Soleimanpour and F. Kanjouri [32] calculated the electronic, structural and optical properties of the cubic perovskite  $\text{BaSnO}_3$  (pristine). They have used the full potential linearized augmented plane wave (FP-LAPW) based on density functional theory (DFT). This approach has been accounted for the exchange and correlation effects by a generalized gradient approximation (GGA) and an orbital independent modified Becke–Johnson (mBJ) potential as coupled with GGA. All these theoretical calculations have revealed an indirect bandgap nature of  $\text{BaSnO}_3$ . But the calculated values are found to be widely varied depending on the utilized approximation. Therefore, it is essential to identify the best DFT calculation that could well correlate with the experimental data. Thus, we have used in this study the first principles calculations with Perdew – Burke – Ernzerhof (GGA-PBE) and TB-mBJ to examine the structural, electronic, and optical properties of  $\text{BaSn}_{1-x}\text{Co}_x\text{O}_3$  ceramics ( $x = 0, 12.5, 25, 37.5$  and  $50\%$ ). This approach was used in several previous works [29], [33]–[35], as it exhibits excellent performance in most applications and yields an accurate bandgap energy, optical absorbance, transmittance and reflectance properties for numerous semiconductor and isolators.

## 2. Calculation methods

DFT (density functional theory) is a very effective technique for studying physical characteristics of materials. All computations in this investigation were performed using full potential linearized augmented plane wave (FP-LAPW) approach, which is based on the density functional theory (DFT) [36] with the WIEN2k package [37]. The exchange-correlation potential is determined using generalized gradient approximation (GGA) [38] and the modified Becke–Johnson (mBJ) [39]. The RMT (radius of the muffin tin) atomic spheres of Ba, Sn, O and Co atoms are 2.5, 2.1, 1.8 and 2.1 a.u, respectively. The cut-off energy is described by the separation between the core and valence states and is chosen at  $-6.0$  Ry.  $R_{\text{MT}}K_{\text{max}}$  equal to 7, where  $R_{\text{MT}}$  is a minimum radius of the muffin tin spheres and  $K_{\text{max}}$  is the largest K-vector for the basic functions in the reciprocal space. The precision of the self-consistent parameter set at 0.0001 Ry. The number of K-points in the irreducible Brillouin zone (IBZ) used is 400 for pure  $\text{BaSnO}_3$  and 300 for the other compositions. We used a

2×2×2 cubic perovskite supercell with 40 atoms (8 Ba atoms, 8 Sn atoms and 24 oxygen atoms) to estimate the effect of Co-doping concentration on the structural, electronic and optical properties of BaSnO<sub>3</sub> material. The doped structures were constructed with Sn atoms replaced by one cobalt atom for 12.5 %, two atoms for 25 %, three atoms for 37.5 % and four atoms for 50 %.

The optical properties of material are defined as the interaction between a solid and electromagnetic radiation. This response can be detailed by the complex dielectric function [40]:

$$\varepsilon(\omega) = \varepsilon_1(\omega) + i\varepsilon_2(\omega) \quad (1)$$

Where  $\varepsilon_1(\omega)$  and  $\varepsilon_2(\omega)$  are the real and imaginary parts of dielectric function, respectively.

$\varepsilon_1(\omega)$  represents the stored energy of a medium or material that is available to be given out,  $\varepsilon_2(\omega)$  explains the absorption ability of this compound. The latter corresponds to transitions between the empty and occupied energy states explained by the following equation:

$$\text{Im}\varepsilon(\omega) = \varepsilon_2(\omega) = \frac{4\pi^2 e^2}{m^2 \omega^2} \sum_{ij} \int \langle i|M|j \rangle^2 f_i(1 - f_j) \delta(E_f - E_i - \hbar\omega) d^3k \quad (2)$$

Where M is the dipole matrix, e and m are the charge and mass of the electron, respectively,

$\omega$  is the frequency of the incident photon,

$f_i$  is the Fermi distribution function of the i state,

$E_i$  is the electronic energy of i state.

The real part of the dielectric function ( $\omega$ ) can be expressed as a function of the imaginary part using the Kramers-Kronig relations [40]:

$$\text{Re}\varepsilon(\omega) = \varepsilon_1(\omega) = 1 + \frac{2}{\pi} P \int_0^\infty \frac{\omega' \varepsilon_2(\omega') d\omega'}{\omega'^2 - \omega^2} \quad (3)$$

where P is the principal value of this integral.

From the real and imaginary parts of the dielectric function, we can determine other optical properties, like reflectance  $R(\omega)$  and the absorption coefficient  $\alpha(\omega)$  using the following relationships [40]:

$$\alpha(\omega) = \sqrt{2} \omega (\sqrt{\varepsilon_1(\omega)^2 + \varepsilon_2(\omega)^2} - \varepsilon_1(\omega))^{\frac{1}{2}} \quad (4)$$

$$R(\omega) = \left| \frac{\sqrt{\varepsilon(\omega)} - 1}{\sqrt{\varepsilon(\omega)} + 1} \right|^2 \quad (5)$$

### 3. Results and discussion

#### 3.1 Structural properties

BaSnO<sub>3</sub> has been reported to crystallize in a cubic perovskite structure with experimental lattice parameters of  $a = b = c = 4.12 \text{ \AA}$  and  $\alpha = \beta = \gamma = 90^\circ$  [15], [26], [27]. The influence of five different Co-doping concentrations on the structural properties of BaSn<sub>1-x</sub>Co<sub>x</sub>O<sub>3</sub> ( $x = 0, 12.5, 25, 37.5$  and  $50 \%$ ) has been analyzed by calculating the total energy as a function of the unit cell volume. This influence has been fitted with Murnaghan's equation (6) of states to obtain the best optimal lattice parameters [41]. The equation is given below:

$$E(V) = E_0 + \left[ \frac{B_0 V}{B'_0 (B'_0 - 1)} \right] \left[ B'_0 \left( 1 - \frac{V_0}{V} \right) + \left( \frac{V_0}{V} \right)^{B'_0} - 1 \right] \quad (6)$$

Where:

$E_0$ , and  $V_0$  are the equilibrium total energy and the volume of the system respectively.

$B_0$ , and  $B'_0$  are the bulk modulus and its derivative at zero pressure respectively.

Figure 1. (a-e) shows the calculated total energies as a function of the cell volumes for Co-doped BaSnO<sub>3</sub> with the different doping rates: a. 0 %, b. 12.5 %, c. 25 %, d. 37.5 % and e. 50 % using GGA approximation. This provided an equilibrium lattice constant of  $4.17 \text{ \AA}$  for pure BaSnO<sub>3</sub> which is around 5 % larger than the reported experimental values [15]–[17]. Figure 1. (f) shows the evolution of the lattice parameter as a function of the five different Co-doping rates. In fact, the lattice parameter linearly decreases with increasing cobalt concentration. The lattice parameters obtained from this study are summarized in table 1 with both experimental and previous theoretical data reported in pertinent literature. According to the calculations, the relaxed lattice parameter for pure BaSnO<sub>3</sub> was found to be  $a = b = c = 4.171 \text{ \AA}$ , which is very close to the experimental values [15]–[17] and almost similar to previous theoretical values [29], [32]. This confirms that the method used in the present study is reliable. Furthermore, the value of lattice parameter for the BaSn<sub>1-x</sub>Co<sub>x</sub>O<sub>3</sub> linearly decreases to become  $4.132 \text{ \AA}$  for 12.5 %,  $4.127 \text{ \AA}$  for 25 %,  $4.091 \text{ \AA}$  for 37.5 % and  $4.069 \text{ \AA}$  for 50 % of

Co-doping rates. This could be mostly attributed to the fact that the ionic radius of Sn element is greater than that of Co element [27], [42]. It is well known that the ionic radius of  $\text{Sn}^{4+}$  in  $\text{ABO}_3$  structure (coordination number: 6) is  $0.830 \text{ \AA}$ , which is larger than that of  $\text{Co}^{2+}$  ( $0.790 \text{ \AA}$ ) and  $\text{Co}^{3+}$  ( $0.685 \text{ \AA}$ ). Therefore, it is highly expected that Co ions could enter into the  $\text{BaSnO}_3$  lattice by replacing  $\text{Sn}^{4+}$  ions, regardless of the valence of Co element. Recently, D.S. Gao et al. observed a similar trend of decrease in the lattice parameter of  $\text{BaSn}_{1-x}\text{Co}_x\text{O}_3$  ( $x = 0, 0.05, 0.10, 0.20, 0.35$  and  $0.50$ ) films [27]. They have reported that with the increase of Co content from  $x = 0.05$  to  $0.50$ , the diffraction peak (200) of  $\text{BaSn}_{1-x}\text{Co}_x\text{O}_3$  gradually shifted towards the high-angle direction. This is a clear indication of the effective substitution of Sn atoms by Co atoms into the  $\text{BaSnO}_3$  lattice structure.

### 3.2 Electronic properties

The electronic properties such as the nature of bonds formed between the different elements, the energy gap type, i.e., direct or indirect, mobility of carriers and other properties can be studied from density of states (DOS). Figure 2a and 2b show the band structure, the total and partial densities of states (TDOS, PDOS) of pure  $\text{BaSnO}_3$ , respectively. We have adopted TB-mBJ approximation method in WIEN2K-code package [35] to calculate the band structure, the total and partial densities of states of pure and Co-doped  $\text{BaSnO}_3$  oxide, with different concentrations (12.5 %, 25 %, 37.5 %, and 50 %) of cobalt. The Fermi level ( $E_F$ ) is set to be located at 0 eV and match with the top of the valence band. As can be seen from Figure 2 (a), the valence band maximum (VBM) and conduction band minimum (CBM) are located at the R and  $\Gamma$  points of the Brillouin zone, respectively, implying that  $\text{BaSnO}_3$  is an indirect bandgap semiconductor. The obtained value of the energy gap is  $E_g = 2.62 \text{ eV}$ . This result is in good agreement with other theoretical reports [29], [32], [43], [44] where  $E_g$  ranges from 2.48 to 2.65 eV. This value is also slightly lower than reported experimental values [15]–[17] where  $E_g$  ranges from 3.1 to 3.4 eV. **Indeed, various experimental parameters have a significant impact on the microstructure of the material, regardless of its form (powder, ceramic, or film), and hence on its electrical and optical properties.** From the band structure constructed in fig. 2b, the total density of states can be divided into four different regions. The first region can be indexed to the electronic states located below -8 eV in the lower part of the valence band. These states mainly consist of Ba-5p and Sn-4d states. The second region can be indexed to the electronic states located between -4 eV and 0 eV, which are derived from the O-2p and Sn-5p states. Here there is a hybridization between O-2p and Sn-5p, suggesting that the O-Sn bond has a covalent character in the  $\text{BaSnO}_3$  oxide. The third region can be

indexed to the electronic states located between 2.6 eV and 6 eV of the conduction band. The electronic states in this region could be mainly derived from Sn-5s states, while O-2s and Sn-5p orbitals have minor contributions to the electronic states. It has been revealed that the Sn-5s states have a lower energy than the corresponding Sn-5p orbitals, which leads to antibonding states at the hybridization with O-2s states. The last region is located between 6 eV and 10 eV, which is predominantly composed by Ba-5d states along with a minor contribution from Ba-6s, Sn-5s, and O-2s states. All the above results are in good agreement with previous studies [29], [32].

Figure 3 (a-d) represents the band structures of  $\text{BaSn}_{1-x}\text{Co}_x\text{O}_3$  for different Co-doping rates: a. 12.5, b. 25, c. 37.5 and d. 50 %. Unlike the pure  $\text{BaSnO}_3$  oxide, for all Co-doped  $\text{BaSnO}_3$  compositions, the valence band maximum (VBM) and conduction band minimum (CBM) are positioned in the  $\Gamma$  point of the Brillouin zone. This indicates that the Co-doped  $\text{BaSnO}_3$  oxide has a direct energy bandgap. Additionally, the Fermi level enters into the valence band. The Co-doped  $\text{BaSnO}_3$  is therefore a p-type degenerate semiconductor [42], [45]–[47]. Moreover, the bandgap value decreases from 2.62 eV for pure  $\text{BaSnO}_3$  to 1.42 eV for 50 % (highest doping concentration) of cobalt. This decrease is significant as it represents a decrease of approximately 45 %. Similar kind of decrease in band gap as a function of Co doping concentration in  $\text{BaSnO}_3$  and  $\text{SrSnO}_3$  systems [27], [48], [49]. The different values of  $E_g$  are presented in Figure 4 in function of the Co concentration.

Figure 5 (a-d) represents the total and partial densities of states of  $\text{BaSn}_{1-x}\text{Co}_x\text{O}_3$  ( $x = 12.5, 25, 37.5$  and  $50\%$ ). From these figures, some remarks can be done: i) Co-3d states appear below the upper part of the valence band and at the bottom of the conduction band as well; ii) there is a strongly hybridized in the valence band maximum between O-2p states and Co-3d states. Besides, a weak hybridization between O-2p states and Sn-5p states has been observed in the VBM; iii) when the concentration of cobalt increases, the participation of Sn-5s in the bottom of the conduction band becomes less important compared to that of Co-3d, which becomes more dominant in the VBM and in the CBM. All of these factors contribute to understanding why cobalt doping lowers bandgap energy of  $\text{BaSnO}_3$ . This also correlates well with experimental findings on  $\text{BaSn}_{1-x}\text{Co}_x\text{O}_3$ , which reveal that the cobalt ions dominate conduction in the material[45].

In the case of pure  $\text{BaSnO}_3$ , the partial density of states (PDOS) shows that the VBM dominantly consists of 5s orbitals of Sn atoms and some contributions from the states of Ba

atoms while CBM composed of overlapping orbitals. From the band structures of Co doped BaSnO<sub>3</sub>, it is apparent that the electronic structure of pure BaSnO<sub>3</sub> is greatly altered with a Co atom doping. The alterations are the appearance of new energy lines at the bottom of the conduction bands and new considerable states in the valence band. These new states are expected to be associated with Co dopant. VBM DOS of doped BaSnO<sub>3</sub> originates from the hybridization between the 2p orbitals of the O atoms and 3d orbitals of the Co atoms. These effects of Co atoms have already been observed on thermoelectric oxides [50]. Moreover, the corresponding peak is gained to be intensive in the DOS graph as the concentration of the dopant increases. Therefore, the strong hybridization between d-orbitals of the dopant cobalt and p-orbitals of the O atoms of BaSnO<sub>3</sub> induced new band lines in VBM and CBM, leading to a possible conversion of the indirect bandgap of BaSnO<sub>3</sub> to direct bandgap. Rizwan et al reported direct band gap converts from the original indirect band gap nature of SrTiO<sub>3</sub> upon doping of a transition metal element copper as observed in the present study [51]. Also this kind of conversion has been simulated on another semiconductor dedicated to optoelectronics [52]. Thus, the transformation from the indirect to direct bandgap will facilitate the passage of the electrons from the VBM to CBM with a minimum of energy and will have a good effect on optical transitions. This property would make this material more efficient for photovoltaic applications.

We have also investigated the electron charge density of pure and Co-doped BaSnO<sub>3</sub> material, with different concentrations (0%, 12.5 %, 25 %, 37.5 %, and 50 %) of cobalt using TB-mBJ approximation. The charge density mapping of these compositions is shown in figure 6 along (110) plane. For pure BaSnO<sub>3</sub>, the contour lines are overlapping between Sn and O atoms. This implies that the bond between Sn and O atoms is covalent, which is due to hybridization between O-2p and Sn-5p states. On the other hand, the contour lines are weakening between Ba and O atoms, indication of ionic bond between these two atoms. It is interesting to note that the covalent bond between Sn and O is gradually weakening upon an increasing in cobalt doping. Simultaneously, the cobalt is forming a covalent bonding with oxygen atoms significantly. Based on the electronegativity differences between Sn and O atoms and between Co and O atoms are found to be 1.56 and 1.48 eV, respectively. This confirms that Sn and Co atoms can form covalent bonding with O atom individually.

### **3.3 Optical properties:**

For photovoltaic cells, verifying the effect of solar radiation on the optical properties of pure and Co-doped BaSnO<sub>3</sub> is essential. Thus, we investigated parameters such as absorption coefficient, optical transmittance, reflectivity, and optical bandgap of pure and Co-doped BaSnO<sub>3</sub> oxide using the TB-mBJ approximation approach.

Figure 7 depicts the optical transmittance spectra of BaSn<sub>1-x</sub>Co<sub>x</sub>O<sub>3</sub> as a function of different Co-doping concentrations (x = 0, 12.5, 25, 37.5 and 50 %). The pure BaSnO<sub>3</sub> has revealed the maximum optical transmittance of about 90 % in the band above 400 nm, while the percentage slightly decreases from 90 % to 85 % in the ultraviolet band, forming the absorption edge. However, the exchange of Sn atoms by Co has resulted in a linear decrease in the transmittance percentage when the Co concentration increases. The optical transmittance percentage slightly decreases in the band above 400 nm when the Co-doping concentration increases from 12.5 to 50 %. The percentages of optical transmittance were found to be around 85 %, 80 %, 75 % and 70 % for Co-doping concentrations of 12.5 %, 25 %, 37.5 % and 50 %, respectively. Likewise, the reflectance percentage has decreased in the UV band, i.e., below 400 nm. Moreover, there was a linear blue shift in the absorption edge, i.e., towards the UV band between 200 and 250 nm. That could be owing to the slight anti-reflection effect induced by the Co-doping, due to the lower refractive index nature of cobalt, in the BaSnO<sub>3</sub> lattice [53]. In short, this decrease in the transmittance upon Co-doping was caused by the increase in light absorption capability upon Co-doping into the BaSnO<sub>3</sub> oxide. A similar kind of behavior has been reported by D.-S. Gao et al. [27] on Co-doped BaSnO<sub>3</sub> thin films grown on MgO single-crystal substrates.

Figure 8 depicts the absorption coefficient spectra of pure and Co-doped BaSnO<sub>3</sub> oxides. The absorption coefficient was measured between 200 and 800 nm. As shown in the spectra, the absorption coefficient was low in the visible band, above 400 nm, for the pure BaSnO<sub>3</sub>. The shallow acceptor states produce enhanced absorption in the visible band with Co ions doping. The transmittance measurements in Fig. 7 are closely associated with this trend. The average transmittance declines in the band of the visible spectrum upon Co-doping, which is in qualitative agreement with the absorption coefficient trend. Upon Co-doping, the absorption coefficient has obviously increased in both the UV and visible bands. Particularly, the absorption coefficient seemingly predominant in the UV band, between 200 and 380 nm. Additionally, there was a net improvement of the absorption coefficient at the beginning of the visible band. The maximum values of the absorption coefficient were of about 10, 20, 30, 45 and 60.10<sup>4</sup>/cm at around 300 nm, for x = 0, 12.5, 25, 37.5 and 50 % of Co-doping

concentration, respectively. The maximum absorption of about  $60.10^4$  /cm in the UV band and  $25.10^4$  /cm at the beginning of the visible band were therefore obtained for 50 % of Co-doping concentration. Thus, this absorption coefficient enhancement by Co-doping confirms that BaSnO<sub>3</sub> can make an efficient system for optoelectronic applications.

**Figure 9** depicts the reflectance spectra of BaSnO<sub>3</sub> as a function of different Co-doping concentrations. The pure BaSnO<sub>3</sub> oxide exhibits a low reflectivity of about 8 % throughout the UV-visible bands (200 – 700 nm). Interestingly, the reflectance percentage was increased upon increasing the Co-doping concentration, with a maximum value of about 25 % around 320 nm for 50 % Co-doping concentration. The reflectivity upon Co-doping was particularly enhanced in the UV band (200 – 380 nm) and at the beginning of the visible band (400 – 550 nm). Around 300 – 350 nm, the reflectance percentage is 9 %, 10 %, 12 % and 14 % for the doping concentration of 12.5 %, 25 %, 37.5 and 50 % respectively. Besides, the reflectance percentage slightly decreased in the 350 – 500 nm band with a maximum reflectance of about 15 % for 50 % Co-doping concentration.

**Figure 10** shows the optical bandgap of BaSnO<sub>3</sub> as a function of different Co-doping concentration using mBJ correction. The optical bandgap energy ( $E_g$ ) of the pure BaSnO<sub>3</sub> oxide was found to be 2.6 eV. The  $E_g$  value has significantly decreased upon Co-doping. Actually, the  $E_g$  values are found to be 2.50, 2.22, 1.49 and 1.35 eV for 12.5 %, 25 %, 37.5 % and 50 % of Co-doping concentration, respectively. Experimental works done on Co-doped BaSnO<sub>3</sub> powder for low doping rate also show a decrease of the optical bandgap energy [28], [48]. Effectively when the doping concentration is increased, the wave functions of the electrons associated with these doping atoms start to overlap [27], [42]. This overlap leads in turn to the formation of an energy band rather than being a discrete level. And finally, this additional energy band decreases the optical energy gap of the host system. Thus, it is highly anticipated that this red shift may be attributed to the formation of new intermediate energy levels due to the Co doping into the BaSnO<sub>3</sub> host lattice. The optical absorption spectra reveal the interaction between the Ba–Sn–O lattice and dopant Co. The decrease in the optical band gap of BaSnO<sub>3</sub> by Co dopant will assist in improving the light absorption efficiency in the visible band of the solar spectrum. And this more efficient absorption will in turn improve the performance of photovoltaic cells.

## Conclusion

In this study, a theoretical investigation of pure and Co doped BaSnO<sub>3</sub> oxides was developed to examine the influence of cobalt (Co) on the structural, electronic, and optical properties of BaSnO<sub>3</sub>. The lattice parameter, both electronic and optical energy bandgap of the doped materials decrease with Co-doping concentration. Moreover, the absorption coefficient and reflectivity increase upon Co-doping. Additionally, this work shows that a direct bandgap could be obtained by doping the BaSnO<sub>3</sub> host with Co. The results yielded by this theoretical study are in good agreement with experimental and theoretical reports. The present approach can therefore contribute to the improvement of device performance of quasi transparent electronic materials, especially in the fields of photovoltaic and optoelectronic devices.

## References

- [1] I. Grinberg, D. V. West, M. Torres, G. Gou, D. M. Stein, L. Wu, G. Chen, E. M. Gallo, A. R. Akbashev, P. K. Davies, J. E. Spanier and A. M. Rappe, 'Perovskite oxides for visible-light-absorbing ferroelectric and photovoltaic materials', *Nature*, vol. 503, no. 7477, pp. 509–512, Nov. 2013, doi: 10.1038/nature12622.
- [2] Ramovatar, I. Coondoo, P. Kumar, A. A. Khan, S. Satapathy, and N. Panwar, 'Observation of large electrocaloric properties in lead-free  $\text{Ba}_{0.98}\text{Ca}_{0.02}\text{Ti}_{0.98}\text{Sn}_{0.02}\text{O}_3$  ceramics', *AIP Adv.*, vol. 9, no. 5, p. 055010, May 2019, doi: 10.1063/1.5091975.
- [3] W.-J. Yin, B. Weng, J. Ge, Q. Sun, Z. Li, and Y. Yan, 'Oxide perovskites, double perovskites and derivatives for electrocatalysis, photocatalysis, and photovoltaics', *Energy Environ. Sci.*, vol. 12, no. 2, pp. 442–462, 2019, doi: 10.1039/C8EE01574K.
- [4] N. Arjun, G.-T. Pan, and T. C. K. Yang, 'The exploration of Lanthanum based perovskites and their complementary electrolytes for the supercapacitor applications', *Results Phys.*, vol. 7, pp. 920–926, 2017, doi: 10.1016/j.rinp.2017.02.013.
- [5] D. O. Scanlon, 'Defect engineering of  $\text{BaSnO}_3$  for high-performance transparent conducting oxide applications', *Phys. Rev. B*, vol. 87, no. 16, p. 161201, Apr. 2013, doi: 10.1103/PhysRevB.87.161201.
- [6] J. Shin, Y. M. Kim, Y. Kim, C. Park, and K. Char, 'High mobility  $\text{BaSnO}_3$  films and field effect transistors on non-perovskite  $\text{MgO}$  substrate', *Appl. Phys. Lett.*, vol. 109, no. 26, p. 262102, Dec. 2016, doi: 10.1063/1.4973205.
- [7] S. Raghavan, T. Schumann, H. Kim, J. Y. Zhang, T. A. Cain, and S. Stemmer, 'High-mobility  $\text{BaSnO}_3$  grown by oxide molecular beam epitaxy', *APL Mater.*, vol. 4, no. 1, p. 016106, Jan. 2016, doi: 10.1063/1.4939657.
- [8] U. Kim, C. Park, T. Ha, Y. M. Kim, N. Kim, C. Ju, J. Park, J. Yu, J. H. Kim and K. Char, 'All-perovskite transparent high mobility field effect using epitaxial  $\text{BaSnO}_3$  and  $\text{LaInO}_3$ ', *APL Mater.*, vol. 3, no. 3, p. 036101, Mar. 2015, doi: 10.1063/1.4913587.

- [9] H. B. Sales, V. Bouquet, S. Députier, S. Ollivier, F. Gouttefangeas, M. Guilloux-Viry, V. Dorcet, I. T. Weber, A. G. d. Souza, I. M. G. d. Santos, 'Sr<sub>1-x</sub>Ba<sub>x</sub>SnO<sub>3</sub> system applied in the photocatalytic discoloration of an azo-dye', *Solid State Sci.*, vol. 28, pp. 67–73, Feb. 2014, doi: 10.1016/j.solidstatesciences.2013.12.007.
- [10] Y. Yuan, J. Lv, X. Jiang, Z. Li, T. Yu, Z. Zou, and J. Ye, 'Large impact of strontium substitution on photocatalytic water splitting activity of BaSnO<sub>3</sub>', *Appl. Phys. Lett.*, vol. 91, no. 9, p. 094107, Aug. 2007, doi: 10.1063/1.2778631.
- [11] Z. Zhang, X. Li, C. Gao, F. Teng, Y. Wang, L. Chen, W. Han, Z. Zhang and E. Xie, 'Synthesis of cadmium sulfide quantum dot-decorated barium stannate nanowires for photoelectrochemical water splitting', *J. Mater. Chem. A*, vol. 3, no. 24, pp. 12769–12776, 2015, doi: 10.1039/C5TA01948F.
- [12] R. A. Bucur, A. I. Bucur, S. Novaconi, and I. Nicoara, 'BaSnO<sub>3</sub> based thermally stable capacitors', *J. Alloys Compd.*, vol. 542, pp. 142–146, Nov. 2012, doi: 10.1016/j.jallcom.2012.07.072.
- [13] A. Roy, P. Selvaraj, P. Sujatha Devi, and S. Sundaram, 'Morphology tuned BaSnO<sub>3</sub> active layer for ambient perovskite solar cells', *Mater. Lett.*, vol. 219, pp. 166–169, May 2018, doi: 10.1016/j.matlet.2018.02.055.
- [14] S. S. Shin et al., 'Colloidally prepared La-doped BaSnO<sub>3</sub> electrodes for efficient, photostable perovskite solar cells', *Science*, vol. 356, no. 6334, pp. 167–171, Apr. 2017, doi: 10.1126/science.aam6620.
- [15] G. Larramona, C. Gutiérrez, I. Pereira, M. R. Nunes, and F. M. A. da Costa, 'Characterization of the mixed perovskite BaSn<sub>1-x</sub>Sb<sub>x</sub>O<sub>3</sub> by electrolyte electroreflectance, diffuse reflectance, and X-ray photoelectron spectroscopy', *J. Chem. Soc. Faraday Trans. 1 Phys. Chem. Condens. Phases*, vol. 85, no. 4, p. 907, 1989, doi: 10.1039/f19898500907.
- [16] H. Mizoguchi, H. W. Eng, and P. M. Woodward, 'Probing the Electronic Structures of Ternary Perovskite and Pyrochlore Oxides Containing Sn<sup>4+</sup> or Sb<sup>5+</sup>', *Inorg. Chem.*, vol. 43, no. 5, pp. 1667–1680, Mar. 2004, doi: 10.1021/ic034551c.
- [17] H. Mizoguchi, P. M. Woodward, C.-H. Park, and D. A. Keszler, 'Strong Near-Infrared Luminescence in BaSnO<sub>3</sub>', *J. Am. Chem. Soc.*, vol. 126, no. 31, pp. 9796–9800, Aug. 2004, doi: 10.1021/ja048866i.
- [18] K. K. James, P. S. Krishnaprasad, K. Hasna, and M. K. Jayaraj, 'Structural and optical properties of La-doped BaSnO<sub>3</sub> thin films grown by PLD', *J. Phys. Chem. Solids*, vol. 76, pp. 64–69, Jan. 2015, doi: 10.1016/j.jpcs.2014.07.024.

- [19] L. Zhu, J. Ye, X. Zhang, H. Zheng, G. Liu, X. Pan, and S. Dai, 'Performance enhancement of perovskite solar cells using a La-doped BaSnO<sub>3</sub> electron transport layer', *J. Mater. Chem. A*, vol. 5, no. 7, pp. 3675–3682, 2017, doi: 10.1039/C6TA09689A.
- [20] A. V. Sanchela, M. Wei, J. Lee, G. Kim, H. Jeon, B. Feng, Y. Ikuhara, H. J. Choa and H. Ohta, 'Buffer layer-less fabrication of a high-mobility transparent oxide semiconductor, La-doped BaSnO<sub>3</sub>', *J. Mater. Chem. C*, vol. 7, no. 19, pp. 5797–5802, 2019, doi: 10.1039/C8TC06177G.
- [21] Z. Wang, H. Paik, Z. Chen, D. A. Muller, and D. G. Schlom, 'Epitaxial integration of high-mobility La-doped BaSnO<sub>3</sub> thin films with silicon', *APL Mater.*, vol. 7, no. 2, p. 022520, Feb. 2019, doi: 10.1063/1.5054810.
- [22] Q. Liu, J. Dai, H. Li, B. Li, Y. Zhang, K. Dai and S. Chen, 'Optical and transport properties of Gd doped BaSnO<sub>3</sub> epitaxial films', *J. Alloys Compd.*, vol. 647, pp. 959–964, Oct. 2015, doi: 10.1016/j.jallcom.2015.06.014.
- [23] U. S. Alaan, P. Shafer, A. T. N'Diaye, E. Arenholz, and Y. Suzuki, 'Gd-doped BaSnO<sub>3</sub>: A transparent conducting oxide with localized magnetic moments', *Appl. Phys. Lett.*, vol. 108, no. 4, p. 042106, Jan. 2016, doi: 10.1063/1.4939686.
- [24] B. Li, Q. Liu, Y. Zhang, Z. Liu, and L. Geng, 'Highly conductive Nb doped BaSnO<sub>3</sub> thin films on MgO substrates by pulsed laser deposition', *J. Alloys Compd.*, vol. 680, pp. 343–349, Sep. 2016, doi: 10.1016/j.jallcom.2016.04.157.
- [25] H. F. Wang, Q. Z. Liu, F. Chen, G. Y. Gao, W. Wu, and X. H. Chen, 'Transparent and conductive oxide films with the perovskite structure: La- and Sb-doped BaSnO<sub>3</sub>', *J. Appl. Phys.*, vol. 101, no. 10, p. 106105, May 2007, doi: 10.1063/1.2736629.
- [26] R. Köferstein and F. Yakuphanoglu, 'Semiconducting properties of Ge-doped BaSnO<sub>3</sub> ceramic', *J. Alloys Compd.*, vol. 506, no. 2, pp. 678–682, Sep. 2010, doi: 10.1016/j.jallcom.2010.07.041.
- [27] D.-S. Gao, X.-D. Gao, Y.-Q. Wu, T.-T. Zhang, J.-N. Yang, and X.-M. Li, 'Epitaxial Co doped BaSnO<sub>3</sub> thin films with tunable optical bandgap on MgO substrate', *Appl. Phys. A*, vol. 125, no. 3, p. 158, Mar. 2019, doi: 10.1007/s00339-019-2466-3.
- [28] N. Rajamanickam, S. Isogami, and K. Ramachandran, 'Effect of Co doping for improved photovoltaic performance of dye-sensitized solar cells in BaSnO<sub>3</sub> nanostructures', *Mater. Lett.*, vol. 275, p. 128139, Sep. 2020, doi: 10.1016/j.matlet.2020.128139.

- [29] A. Slassi, 'Ab initio study of a cubic perovskite: Structural, electronic, optical and electrical properties of native, lanthanum- and antimony-doped barium tin oxide', *Mater. Sci. Semicond. Process.*, vol. 32, pp. 100–106, Apr. 2015, doi: 10.1016/j.mssp.2014.12.031.
- [30] Y. Wang, R. Sui, M. Bi, W. Tang, and S. Ma, 'Strain sensitivity of band structure and electron mobility in perovskite  $\text{BaSnO}_3$ : first-principles calculation', *RSC Adv.*, vol. 9, no. 25, pp. 14072–14077, 2019, doi: 10.1039/C9RA02146A.
- [31] J. Cuervo Farfán, J. Arbey Rodríguez, F. Fajardo, E. Vera López, D. A. Landínez Téllez, and J. Roa-Rojas, 'Structural properties, electric response and electronic feature of perovskite', *Phys. B Condens. Matter*, vol. 404, no. 18, pp. 2720–2722, Oct. 2009, doi: 10.1016/j.physb.2009.06.126.
- [32] S. Soleimanpour and F. Kanjouri, 'First principle study of electronic and optical properties of the cubic perovskite  $\text{BaSnO}_3$ ', *Phys. B Condens. Matter*, vol. 432, pp. 16–20, Jan. 2014, doi: 10.1016/j.physb.2013.09.004.
- [33] F. Tran and P. Blaha, 'Accurate Band Gaps of Semiconductors and Insulators with a Semilocal Exchange-Correlation Potential', *Phys. Rev. Lett.*, vol. 102, no. 22, p. 226401, Jun. 2009, doi: 10.1103/PhysRevLett.102.226401.
- [34] S. Chen, X. G. Gong, A. Walsh, and S.-H. Wei, 'Crystal and electronic band structure of  $\text{Cu}_2\text{ZnSnX}_4$  ( $X=\text{S}$  and  $\text{Se}$ ) photovoltaic absorbers: First-principles insights', *Appl. Phys. Lett.*, vol. 94, no. 4, p. 041903, Jan. 2009, doi: 10.1063/1.3074499.
- [35] H. Dixit, R. Saniz, S. Cottenier, D. Lamoen, and B. Partoens, 'Electronic structure of transparent oxides with the Tran–Blaha modified Becke–Johnson potential', *J. Phys. Condens. Matter*, vol. 24, no. 20, p. 205503, May 2012, doi: 10.1088/0953-8984/24/20/205503.
- [36] W. Kohn and L. J. Sham, 'Self-Consistent Equations Including Exchange and Correlation Effects', *Phys. Rev.*, vol. 140, no. 4A, pp. A1133–A1138, Nov. 1965, doi: 10.1103/PhysRev.140.A1133.
- [37] P. Blaha, K. Schwarz, G. K. Madsen, D. Kvasnicka, and J. Luitz, 'wien2k', *Augment. Plane Wave Local Orbitals Program Calc. Cryst. Prop.*, 2001.
- [38] J. P. Perdew, K. Burke, and M. Ernzerhof, 'Generalized Gradient Approximation Made Simple', *Phys. Rev. Lett.*, vol. 77, no. 18, pp. 3865–3868, Oct. 1996, doi: 10.1103/PhysRevLett.77.3865.

- [39] D. Koller, F. Tran, and P. Blaha, ‘Merits and limits of the modified Becke-Johnson exchange potential’, *Phys. Rev. B*, vol. 83, no. 19, p. 195134, May 2011, doi: 10.1103/PhysRevB.83.195134.
- [40] C. Ambrosch-Draxl and J. O. Sofo, ‘Linear optical properties of solids within the full-potential linearized augmented planewave method’, *Comput. Phys. Commun.*, vol. 175, no. 1, pp. 1–14, Jul. 2006, doi: 10.1016/j.cpc.2006.03.005.
- [41] V. G. Tyuterev and N. Vast, ‘Murnaghan’s equation of state for the electronic ground state energy’, *Comput. Mater. Sci.*, vol. 38, no. 2, pp. 350–353, Dec. 2006, doi: 10.1016/j.commatsci.2005.08.012.
- [42] S. Sumithra and N. V. Jaya, ‘Tunable Optical Behaviour and Room Temperature Ferromagnetism of Cobalt-Doped BaSnO<sub>3</sub> Nanostructures’, *J. Supercond. Nov. Magn.*, vol. 31, no. 9, pp. 2777–2787, Sep. 2018, doi: 10.1007/s10948-017-4504-8.
- [43] B. G. Kim, J. Y. Jo, and S. W. Cheong, ‘Hybrid functional calculation of electronic and phonon structure of BaSnO<sub>3</sub>’, *J. Solid State Chem.*, vol. 197, pp. 134–138, Jan. 2013, doi: 10.1016/j.jssc.2012.08.047.
- [44] D. O. Scanlon, ‘Defect engineering of BaSnO<sub>3</sub> for high-performance transparent conducting oxide applications’, *Phys. Rev. B*, vol. 87, no. 16, p. 161201, Apr. 2013, doi: 10.1103/PhysRevB.87.161201.
- [45] O. Parkash, D. Kumar, K. K. Srivastav, and R. K. Dwivedi, ‘Electrical conduction behaviour of cobalt substituted BaSnO<sub>3</sub>’, *J. Mater. Sci.*, vol. 36, no. 24, pp. 5805–5810, Dec. 2001, doi: 10.1023/A:1012904021501.
- [46] M. Yasukawa, Y. Hamada, T. Kono, K. Ueda, H. Yanagi, S. W. Kim, and H. Hosono, ‘Thermoelectric Properties of P-Type BaSnO<sub>3</sub> Ceramics Doped with Cobalt’, *J. Jpn. Soc. Powder Powder Metall.*, vol. 58, no. 3, pp. 149–154, 2011, doi: 10.2497/jjspm.58.149.
- [47] W.-J. Lee, H. J. Kim, J. Kang, D. H. Jang, T. H. Kim, J. H. Lee, and K. H. Kim, ‘Transparent Perovskite Barium Stannate with High Electron Mobility and Thermal Stability’, *Annu. Rev. Mater. Res.*, vol. 47, no. 1, pp. 391–423, Jul. 2017, doi: 10.1146/annurev-matsci-070616-124109.
- [48] X. Hu, X. Gao, D. Gao, and X. Li, ‘Room-temperature ferromagnetism and oxygen pressure-dependent optical, ferromagnetic properties in SrSn<sub>0.5</sub>Co<sub>0.5</sub>O<sub>3</sub> thin films’, *Mater. Res. Lett.*, vol. 6, no. 5, pp. 276–282, May 2018, doi: 10.1080/21663831.2018.1446055.

- [49] X.-M. Hu, X-D. GAO, X-M. LI, Z-Y. GU, Y. SHI and Y-Q. WU, 'Microstructure and Band Gap Modulation of  $\text{SrSn}_{1-x}\text{Co}_x\text{O}_3$  Epitaxial Thin Films via Pulsed Laser Deposition', *Acta Phys.-Chim. Sin.*, vol. 32, no. 4, pp. 828–833, 2016, doi: 10.3866/PKU.WHXB201603013.
- [50] P. Wei, W. Zhao, D. Tang, W. Zhu, X. Nie, and Q. Zhang, 'On the relevance between fine structure and enhanced performance of skutterudite thermoelectric materials: X-ray spectroscopy studies', *J. Materiomics*, vol. 2, no. 3, pp. 280–289, Sep. 2016, doi: 10.1016/j.jmat.2016.06.001.
- [51] M. Rizwan, A. Ali, Z. Usman, N. R. Khalid, H. B. Jin, and C. B. Cao, 'Structural, electronic and optical properties of copper-doped  $\text{SrTiO}_3$  perovskite: A DFT study', *Phys. B Condens. Matter*, vol. 552, pp. 52–57, Jan. 2019, doi: 10.1016/j.physb.2018.09.022.
- [52] B. Sainbileg and M. Hayashi, 'Possible indirect to direct bandgap transition in  $\text{SnS}_2$  via nickel doping', *Chem. Phys.*, vol. 522, pp. 59–64, Jun. 2019, doi: 10.1016/j.chemphys.2019.02.014.
- [53] E. Amin-Chalhoub, T. Duguet, D. Samélor, O. Debieu, E. Ungureanu, and C. Vahlas, 'Chemical vapor deposition of low reflective cobalt (II) oxide films', *Appl. Surf. Sci.*, vol. 360, pp. 540–546, Jan. 2016, doi: 10.1016/j.apsusc.2015.10.188.

**Table 1**

|              | Percentage of Co concentration (%) | Lattice parameter a (Å) | Reference  |
|--------------|------------------------------------|-------------------------|------------|
| Experimental | Pure BaSnO <sub>3</sub>            | 4.12                    | [25]– [27] |
| Theoretical  | Pure BaSnO <sub>3</sub>            | 4.157                   | [32]       |
| GGA+mBJ      | Pure BaSnO <sub>3</sub>            | 4.17                    | This work  |
| GGA+mBJ      | 12.5                               | 4.13                    | This work  |
|              | 25                                 | 4.12                    |            |
|              | 37.5                               | 4.09                    |            |
|              | 50                                 | 4.06                    |            |
| Experimental | 10                                 | 4.09                    | [27]       |
|              | 20                                 | 4.07                    |            |
|              | 35                                 | 4.03                    |            |
|              | 50                                 | 3.98                    |            |

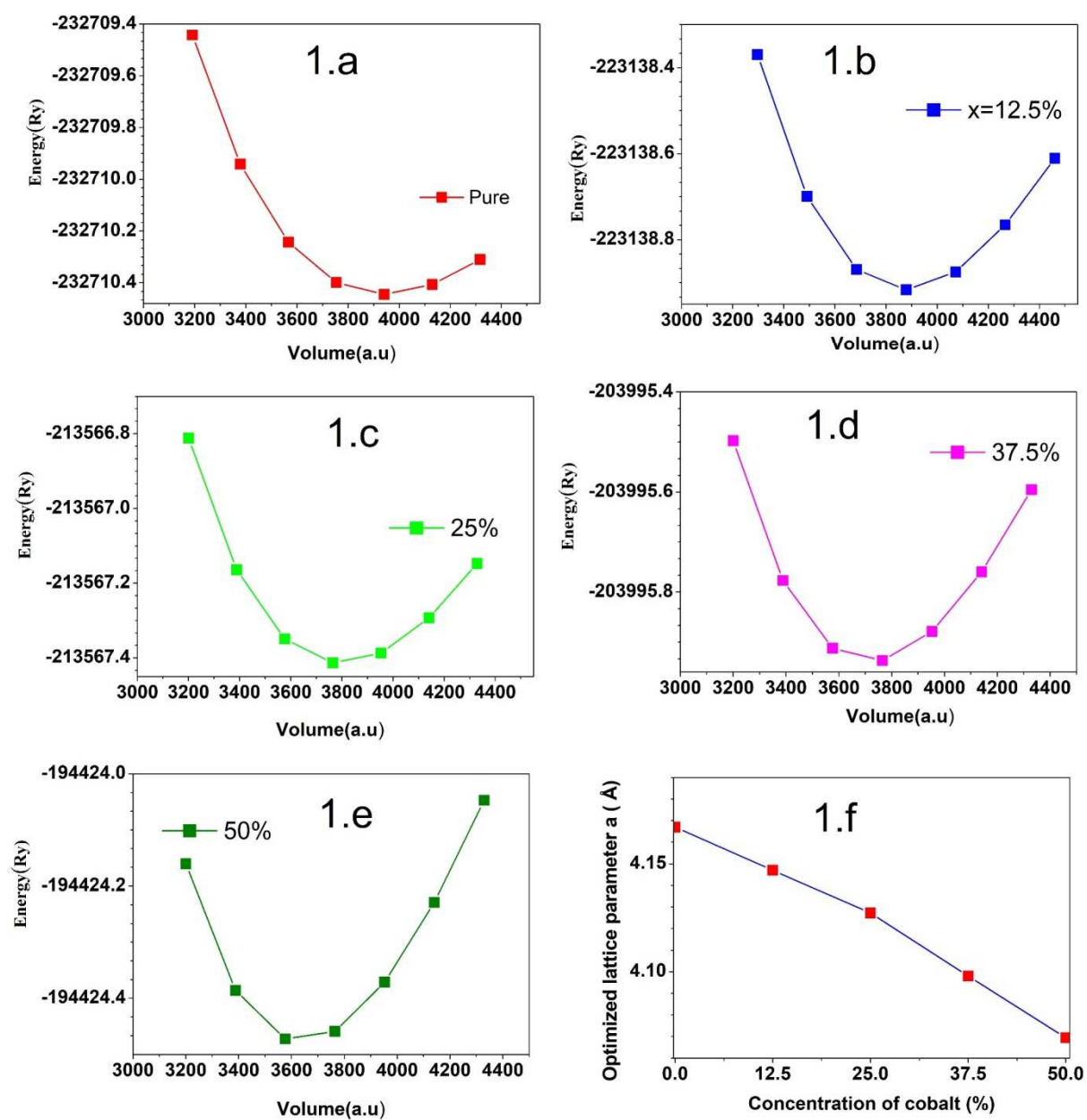
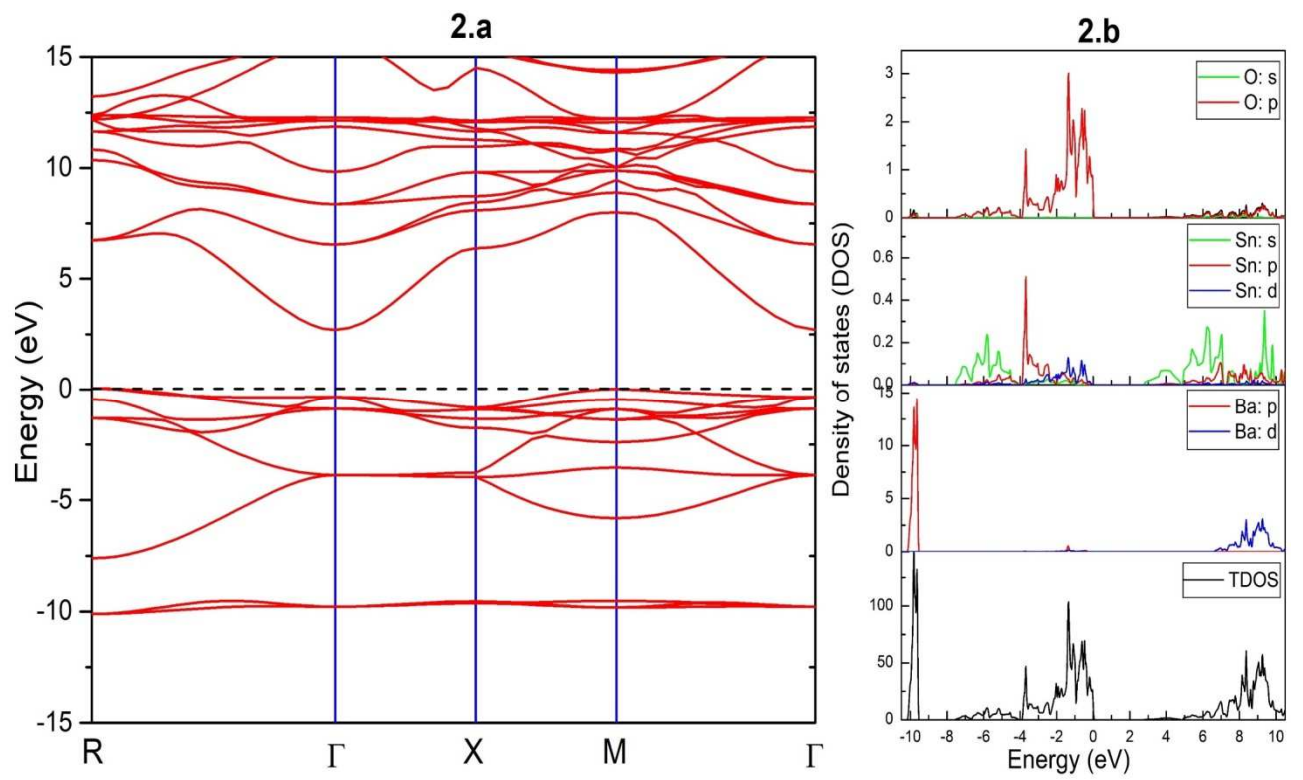
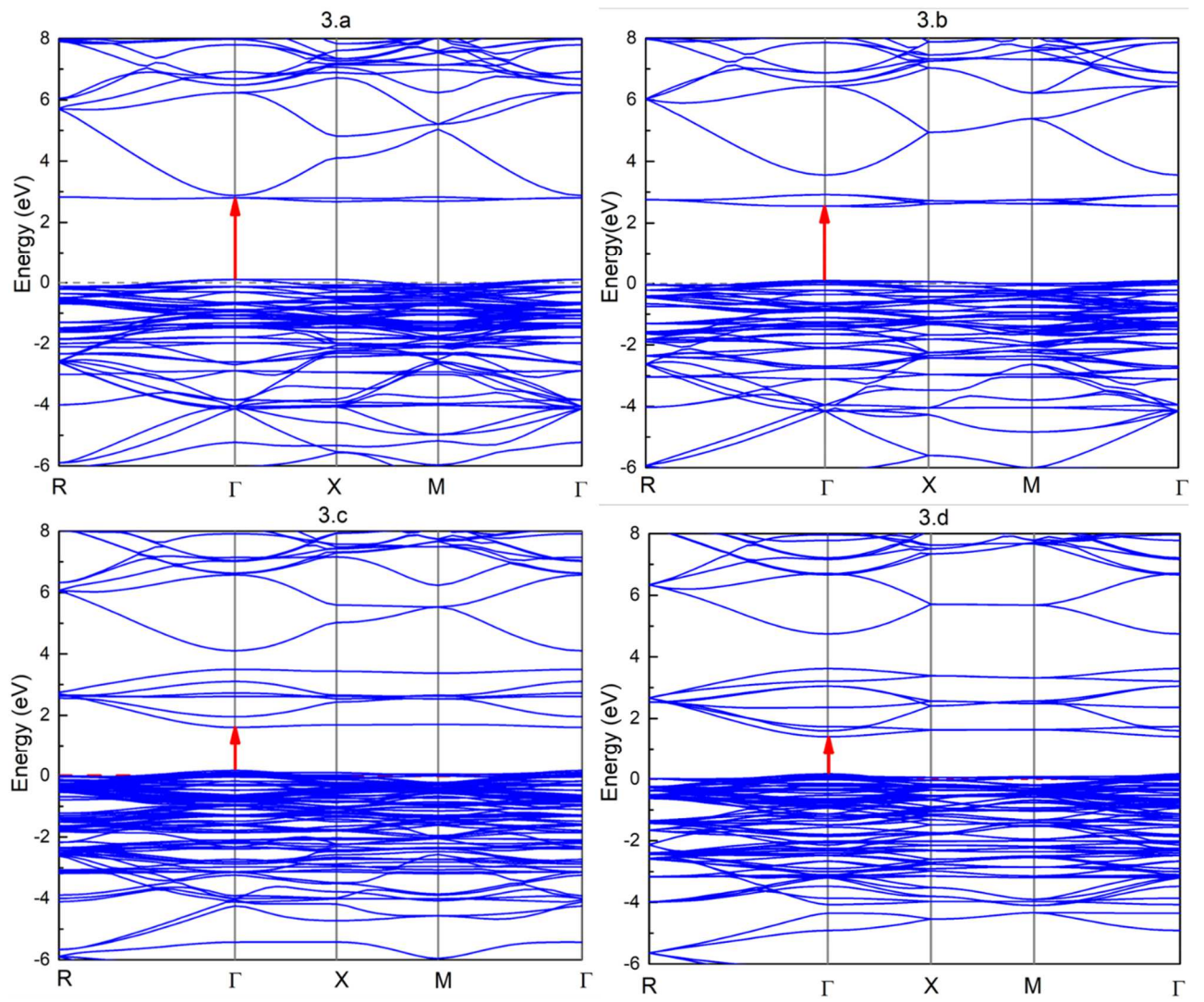


Figure 1



**Figure 2**



**Figure 3**

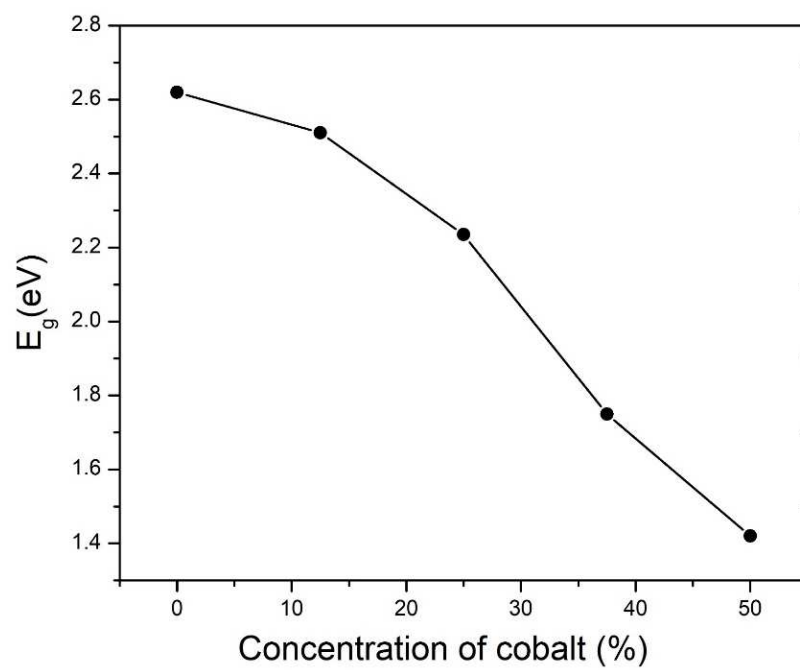


**Figure 4**

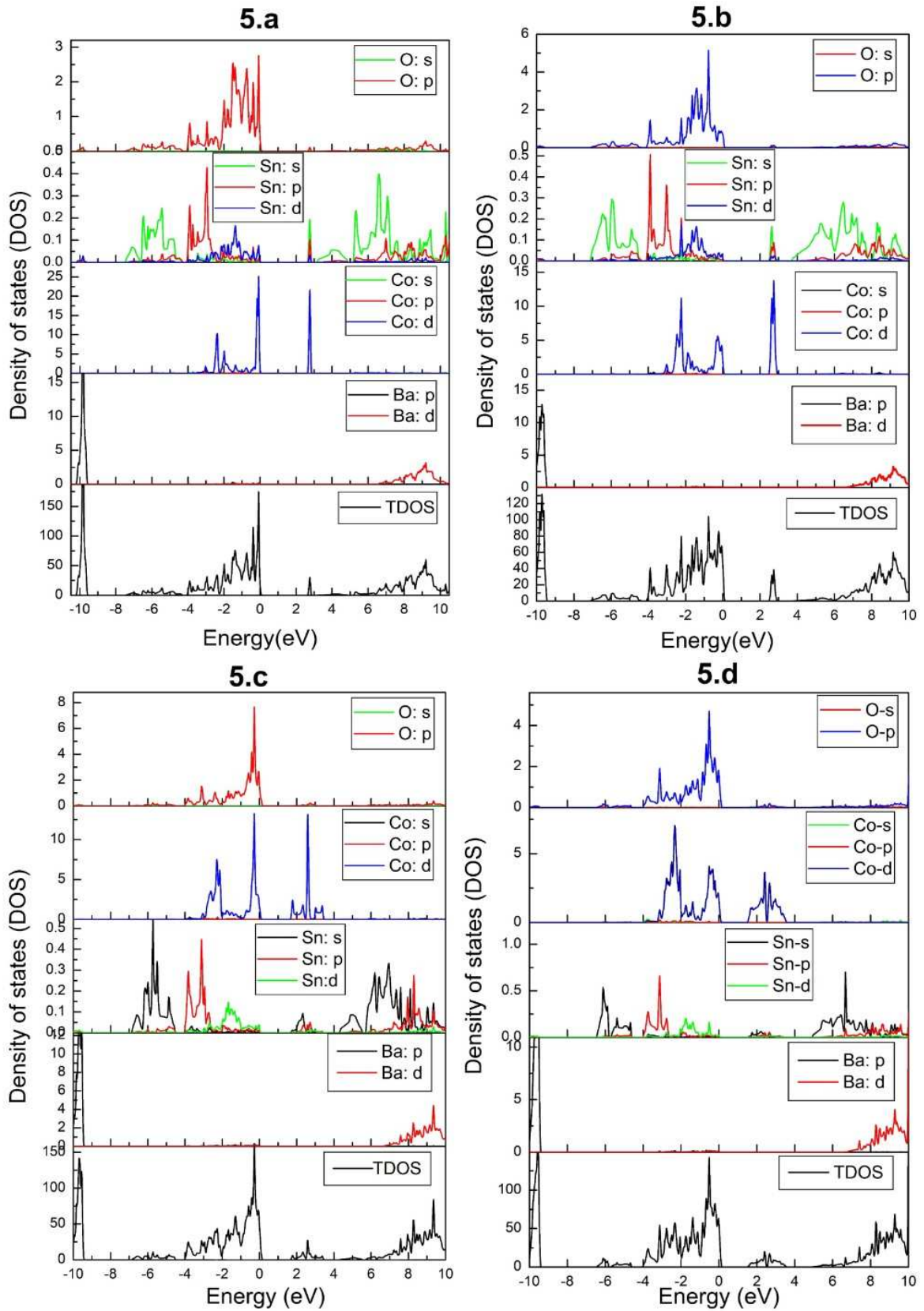
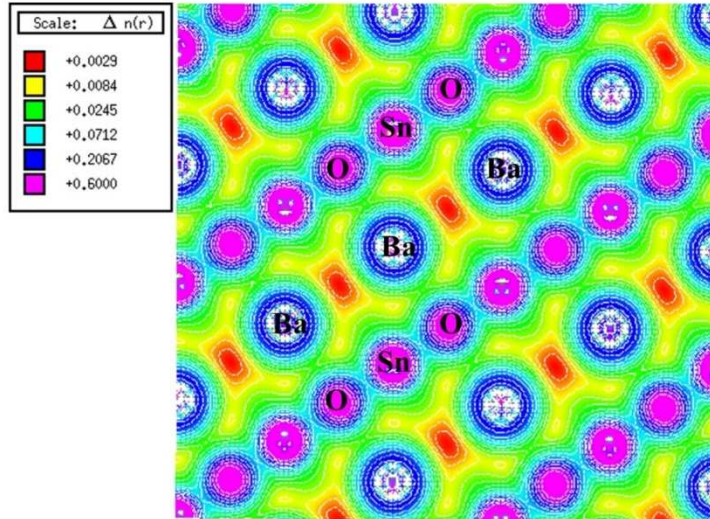
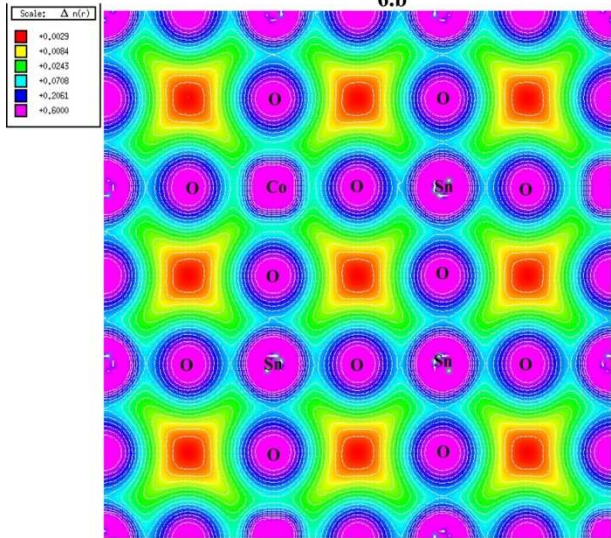


Figure 5

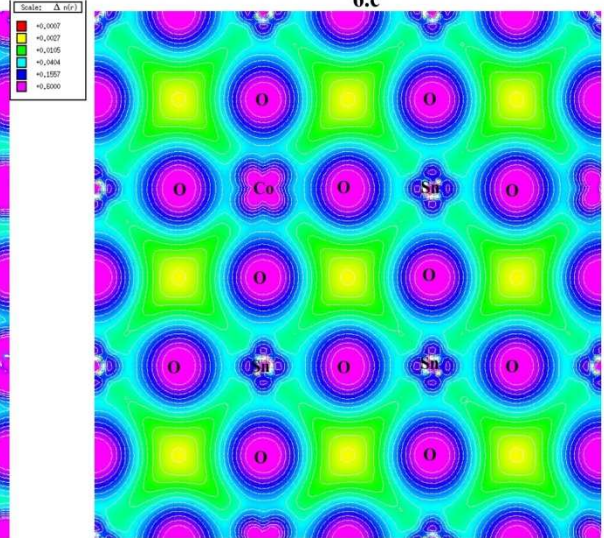
6.a



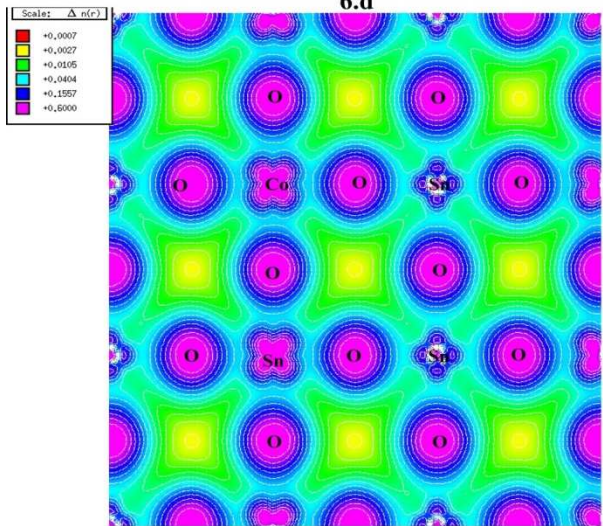
6.b



6.c



6.d



6.e

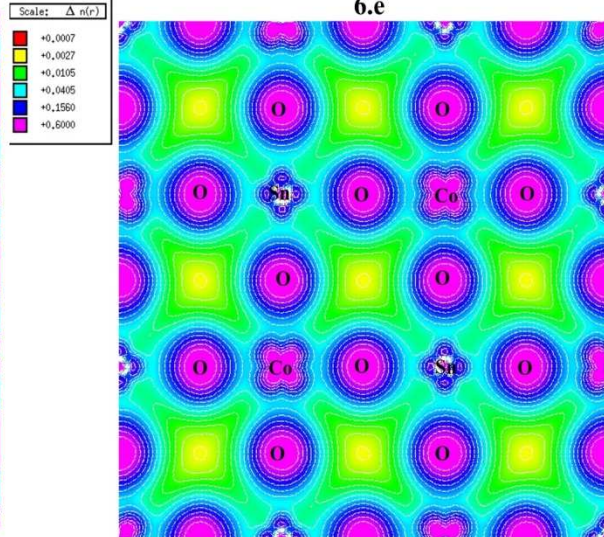
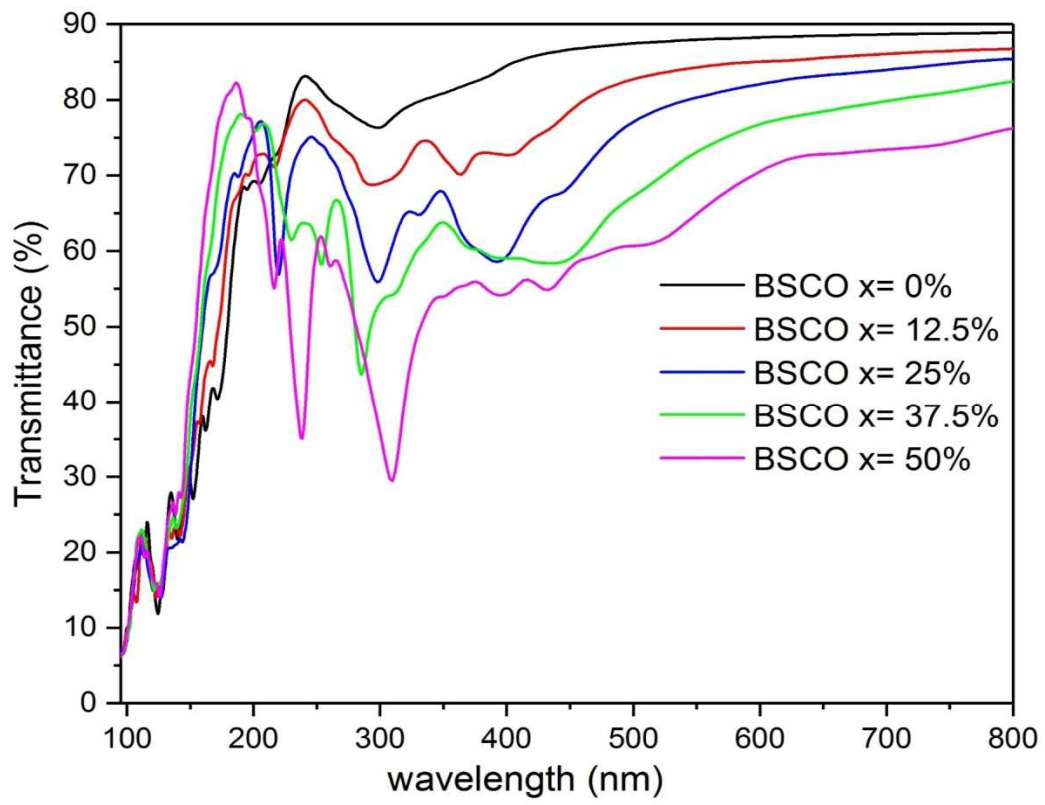
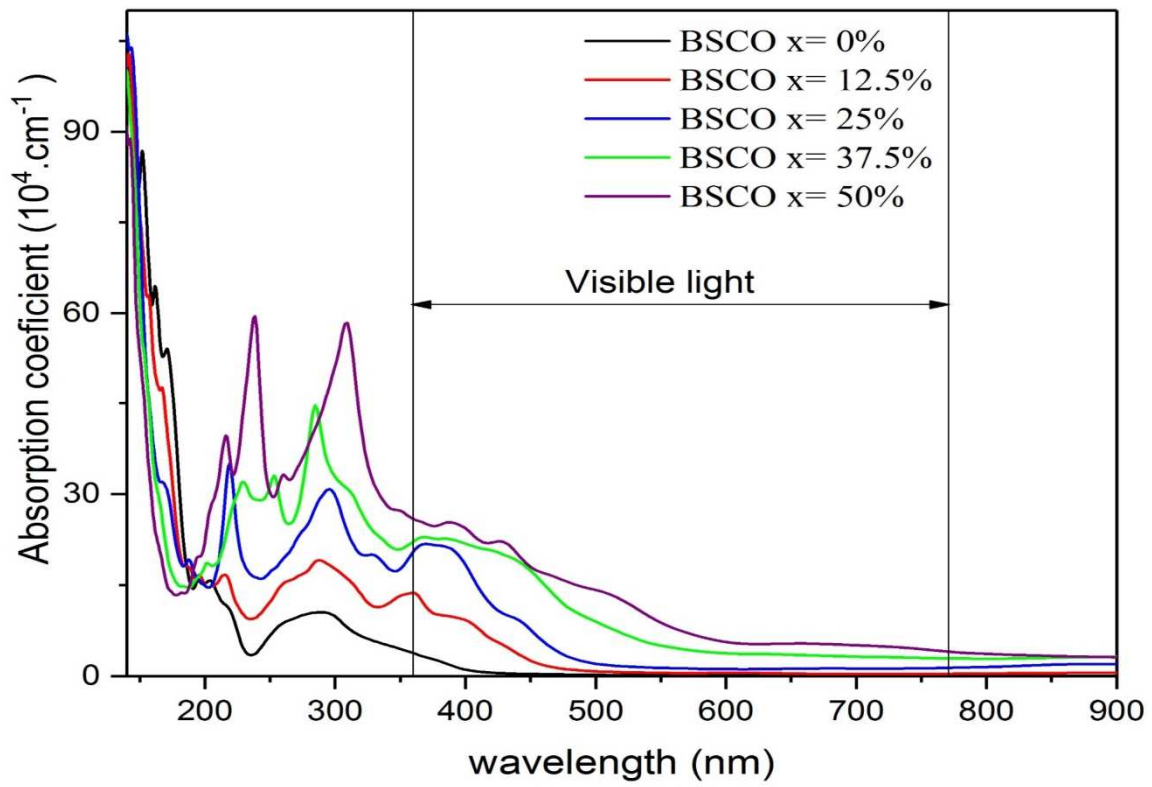


Figure 6



**Figure 7**



**Figure 8**

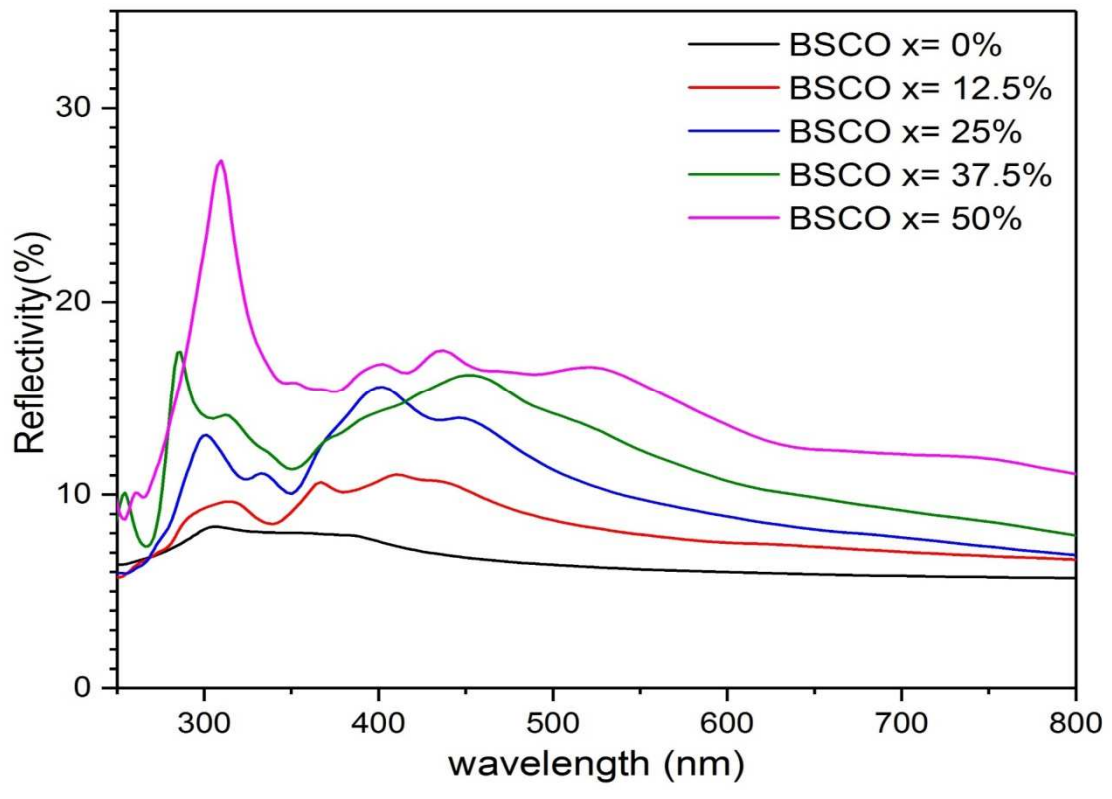


**Figure 9**

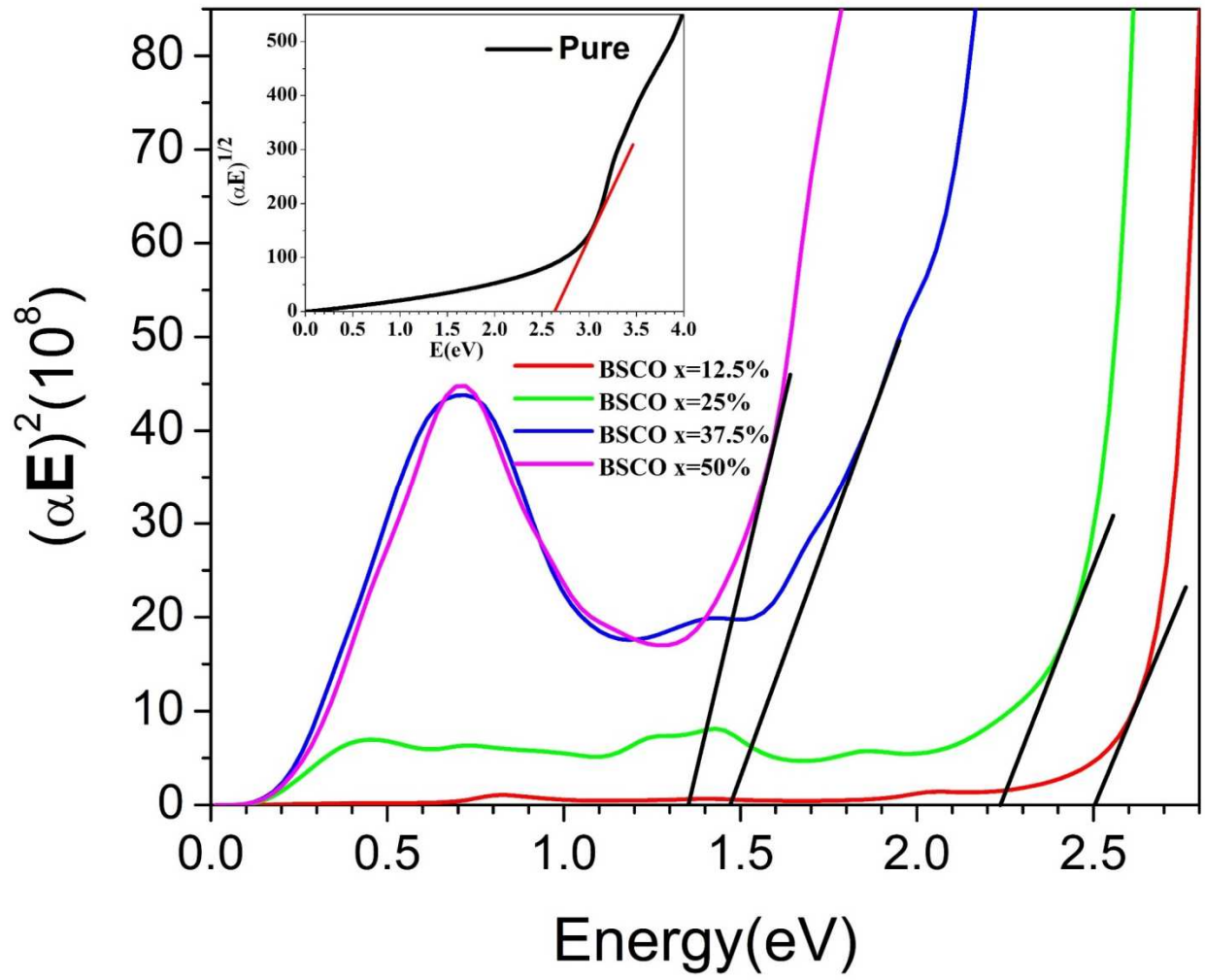


**Figure 10**

**Table caption:**

Table 1. Theoretical and experimental lattice parameter of undoped and Co-doped BaSnO<sub>3</sub>

### Figure captions:

Figure 1. Calculated total energies as a function of the cell volumes for Co-doped BaSnO<sub>3</sub> at (a) 12.5 %, (b) 25 %, (c) 37.5 % and (d) 50 % using GGA approximation, Evolution of lattice parameter of BaSnO<sub>3</sub> as function of Co concentration (f).

Figure 2. (a) The band structure and (b) the total and partial densities of states of pure BaSnO<sub>3</sub>.

Figure 3. Band structure of BaSn<sub>1-x</sub>Co<sub>x</sub>O<sub>3</sub> for different Co-doping rates: (a) 12.5 %, (b) 25 %, (c) 37.5 % and (d) 50 %.

Figure 4. Evolution of the electronic band gap as a function of the Co concentration.

Figure 5. Total and partial densities of Co-doped BaSnO<sub>3</sub> with different Co-doping rates: (a) 12.5 %, (b) 25 %, (c) 37.5 % and (d) 50 %; using TB-mBJ approximation.

Figure 6. Electron charge density distribution of Co-doped BaSnO<sub>3</sub> with different Co-doping rates: (a) 0 %, (b) 12.5 %, (c) 25 %, (d) 37.5 % and (e) 50 %; using TB-mBJ approximation.

Figure 7. Transmittance spectra of BaSn<sub>1-x</sub>Co<sub>x</sub>O<sub>3</sub> (x = 0, 12.5, 25, 37.5 and 50 %).

Figure 8. Absorption coefficient spectra of BaSn<sub>1-x</sub>Co<sub>x</sub>O<sub>3</sub> (x=0, 12.5, 25, 37.5 and 50 %).

Figure 9. Reflectivity spectra of BaSn<sub>1-x</sub>Co<sub>x</sub>O<sub>3</sub> (x=0, 12.5, 25, 37.5 and 50 %).

Figure 10. Optical bandgap of BaSn<sub>1-x</sub>Co<sub>x</sub>O<sub>3</sub> as a function of different Co-doping concentration using mBJ correction.